An Extended Algebraic Reconstruction Technique (E-ART) for Dual Spectral CT

Yunsong Zhao, Xing Zhao, and Peng Zhang*

***Abstract*—Compared with standard computed tomography (CT), dual spectral CT (DSCT) has many advantages for object separation, contrast enhancement, artifact reduction, and material composition assessment. But it is generally difficult to reconstruct images from polychromatic projections acquired by DSCT, because of the nonlinear relation between the polychromatic projections and the images to be reconstructed. This paper first models the DSCT reconstruction problem as a nonlinear system problem; and then extend the classic ART method to solve the nonlinear system. One feature of the proposed method is its flexibility. It fits for any scanning configurations commonly used and does not require consistent rays for different X-ray spectra. Another feature of the proposed method is its high degree of parallelism, which means that the method is suitable for acceleration on GPUs (graphic processing units) or other parallel systems. The method is validated with numerical experiments from simulated noise free and noisy data. High quality images are reconstructed with the proposed method from the polychromatic projections of DSCT. The reconstructed images are still satisfactory even if there are certain errors in the estimated X-ray spectra.**

***Index Terms*—Algebraic reconstruction technique (ART) method, basis material decomposition, Dual spectral CT.**

I. Introduction

In STANDARD computed tomography (CT), the object is scanned under a single X-ray spectrum. The reconstructed CT values are related to the materials and the densities of the scanned object, as well as the X-ray spectrum. Different materials, such as iodinated contrast materials and bone tissues [1], may have similar CT values. This is the reason why standard CT cannot distinguish some materials. However, in dual spectral CT [DSCT, also referred to as dual energy CT (DECT)], the object is scanned under two different X-ray spectra. The DSCT data, which include more information about the scanned object, can be used to reconstruct energy-selective images, images of the electron density and the effective atomic number, or material-selective images [2]–[6]. Therefore the distinguishability of DSCT is remarkably higher than that of standard CT. DSCT has wide potential applications, such as bone mineral density and liver iron concentrations measurements, PET attenuation correction, bone marrow composition analysis, rock core characterization for petrochemical industry, nondestructive evaluation, security inspection, and so forth [7], [8].

Studies on image reconstruction methods for DSCT started in the 1970s. The existing reconstruction methods can be classified into three classes: image based methods, raw data based methods, and iterative methods.

In image based methods, two basis material images are approximated by linear combinations of the two images reconstructed from the two polychromatic DSCT projections separately. Such basis material images are usually regarded as a first-order approximation of the true images. Generally, beam hardening artifacts from reconstruction methods based on monochromatic model [9], [10] propagate into basis material images.

In raw data based methods, two sets of projections of basis material images are obtained from the two polychromatic projections. Then the basis material images are reconstructed from their projections with common image reconstruction methods, such as the filtered backprojection (FBP) method [11] or the backprojection filtration method (BPF) [12]. Generally, raw data based methods can obtain better images than image based methods. But raw data based methods require the DSCT data sets to be geometrically consistent, in other words, two flux measurements corresponding to the low and high X-ray spectra respectively need to be acquired along each X-ray path [13]. However, this requirement is hard to meet for practical DSCT systems, such as dual-source-detector CT systems [14], [15].

Several nonlinear optimization based iterative methods for the DSCT were proposed in [16]–[18]. These methods fit for both geometrically consistent and inconsistent projections. But these methods usually have huge computational costs. An image based iterative method for material decomposition from inconsistent rays (MDIR) was proposed by Maaß *et al.* in [19]. In the iterative process of this method, two basis material images are initialized by the images obtained from an image based method, and

Manuscript received October 12, 2014; revised November 16, 2014; accepted November 17, 2014. Date of publication November 24, 2014; date of current version February 27, 2015. This work was supported in part by the National Natural Science Foundation of China under Grant 61127003, Grant 61371195, and Grant 61401289, and in part by the Beijing Education Committee under Grant PHR20110509 and Grant KZ201110028034. *Asterisk indicates corresponding author.*

Y. Zhao is with the School of Mathematical Sciences, Capital Normal University, Beijing 100048, China, and also with Beijing Higher Institution Engineering Research Center of Testing and Imaging, Beijing 100048, China, and also with the Beijing Center for Mathematics and Information Interdisciplinary Sciences (BCMIIS), Beijing 100048, China, and also with the Shenzhen ZhongKe TianYue Technology Co., Ltd and Shenzhen Institute of Advanced Technology, Shenzhen 518172, China (e-mail: zhao_yunsong@163.com).

X. Zhao is with the School of Mathematical Sciences, Capital Normal University, Beijing 100048, China, and also with Beijing Higher Institution Engineering Research Center of Testing and Imaging, Beijing 100048, China, and also with the Beijing Center for Mathematics and Information Interdisciplinary Sciences (BCMIIS), Beijing 100048, China (e-mail: zhaoxing_1999@126.com).

*P. Zhang is with the School of Mathematical Sciences, Capital Normal University, Beijing 100048, China, and also with Beijing Higher Institution Engineering Research Center of Testing and Imaging, Beijing 100048, China, and also with the Beijing Center for Mathematics and Information Interdisciplinary Sciences (BCMIIS), Beijing 100048, China (e-mail: pzhangct@sina.com).

Color versions of one or more of the figures in this paper are available online at http://ieeexplore.ieee.org.

Digital Object Identifier 10.1109/TMI.2014.2373396

then updated each time by adding the differences between the images reconstructed from the polychromatic projections of the current images and those reconstructed from the measured polychromatic projections. Although the convergence of the MDIR method is not proved theoretically, numerical results show that the qualities of the images reconstructed with the MDIR method are improved much more than that with image based methods. However, there are some artifacts in the images reconstructed with the MDIR method, especially when the angle sampling rate of the polychromatic projections is not large enough.

In this paper, we first model the DSCT reconstruction problem as a nonlinear system problem; and then propose an extended algebraic reconstruction technique (E-ART) to solve the nonlinear system. The proposed E-ART method combines an accurate polychromatic forward projection with a linearized backprojection. The accurate polychromatic forward projection step guarantees that the polychromatic projections of the reconstructed images converge to the measured projections; the linearization in backprojection simplifies the allocation of the residuals. One feature of the proposed method is its flexibility. It fits for any scanning configurations commonly used and does not require consistent rays for different X-ray spectra. Another feature of the proposed method is its high degree of parallelism, which means that the method is suitable for acceleration on GPUs (graphic processing units) or other parallel systems. In this paper, we have restrict our discussion in the case with two spectra and two basis materials. The proposed method can be generalized to multiple spectral CT, such as slow kVp switching CT [20] and photon counting CT [21], and multiple basis material decomposition case [22], without substantial difficulties.

The method is validated with numerical experiments from simulated noise free and noisy data. High quality images are reconstructed with the proposed E-ART method from the polychromatic projections of DSCT. The reconstructed images are still satisfactory even if there are certain errors in the estimated X-ray spectra.

The remainder of this paper is organized as follows. In Section II, we introduce the physical model of DSCT. In Section III, we first propose a model to depict the DSCT reconstruction problem; and then derive the E-ART method for solving the problem. In Section IV, numerical experiments are carried out to verify the proposed method. Finally, we summarize the paper in Section V.

II. DSCT Physical Model

Omitting scattered photons, DSCT reconstruction problem can be boiled down to solving $\mu(\boldsymbol{x}, E)$ from known polychromatic projections [23]

$$p_k(L) = -\ln \int S_k(E) e^{-\int_L \mu(\boldsymbol{x},E)\, dl}\, dE, \quad L \in \mathcal{L}_k, k = 1, 2 \quad (1)$$

where L is an X-ray path and $\mathcal{L}_k$ is the set of X-ray paths corresponding to the kth spectrum; $\mu(\boldsymbol{x}, E)$ is the linear attenuation coefficient of the scanned object at point $\boldsymbol{x} = (x_1, x_2, x_3)$ and energy E; $S_k(E)$ is the kth normalized effective spectrum, which presents compositive effect of the emission spectrum of the X-ray tube, the material and thickness of the detector scintillator, the material and thickness of the filter, etc.

In order to solve (1), $\mu(\boldsymbol{x}, E)$ is usually decomposed as

$$\mu(\boldsymbol{x}, E) = \phi(E) f(\boldsymbol{x}) + \theta(E) g(\boldsymbol{x}) \quad (2)$$

where $\phi(E)$ and $\theta(E)$ are two energy dependent functions, and $f(\boldsymbol{x})$ and $g(\boldsymbol{x})$ are two functions of spatial positions. Typical decomposition methods include photoelectric/Compton effect based decomposition and basis material decomposition. In photoelectric/Compton effect based decomposition, we have $\phi(E) = E^{-3}, \theta(E) = f_{KN}(E)$, where $f_{KN}(E)$ is the Klein-Nishina function. Then $\phi(E) f(\boldsymbol{x})$ and $\theta(E) g(\boldsymbol{x})$ indicate the photoelectric part and the Compton scattering part of the attenuation, respectively. The reconstructed $f(\boldsymbol{x})$ and $g(\boldsymbol{x})$ represent the distributions of the cross sections of these two effects respectively. In basis material decomposition method, $\phi(E)$ and $\theta(E)$ represent the mass attenuation coefficients of the two selected basis materials. The reconstructed $f(\boldsymbol{x})$ and $g(\boldsymbol{x})$ represent the densities of the two basis materials of the scanned object. From the reconstructed $f(\boldsymbol{x})$ and $g(\boldsymbol{x})$ we can also calculate the distributions of the electron density and the effective atomic number of the scanned object.

Substituting (2) into (1), we have

$$p_k(L) = -\ln \int S_k(E) e^{-\phi(E)\int_L f(\boldsymbol{x})\, dl - \theta(E)\int_L g(\boldsymbol{x})\, dl}\, dE, \quad L \in \mathcal{L}_k, k = 1, 2. \quad (3)$$

Now the DSCT reconstruction problem can be expressed as solving $f(\boldsymbol{x})$ and $g(\boldsymbol{x})$ from $p_k(L), L \in \mathcal{L}_k, k = 1, 2$.

In this paper, we assume that $S_k(E)$, $\phi(E)$, and $\theta(E)$ are known. For the estimation of $S_k(E)$ and the measurement of $\phi(E)$ and $\theta(E)$, please refer to [24]–[27].

III. E-ART Method for DSCT

In this section, we first propose a model that depicts the DSCT reconstruction problem; and then derive our E-ART for solving the problem. Since the proposed method is inspired by the classic ART method [28], a short review of the ART method is also given.

A. Discrete Model of DSCT

Consider the discrete form of (3). Divide the valid energy range of the kth X-ray spectrum into M_k parts with δ length subinterval. Suppose that $S_{k,m}$, ϕ_m, and θ_m are the sampling values of $S_k(E)$, $\phi(E)$, and $\theta(E)$ in the mth subinterval, then we get the discrete form of $S_k(E)$, $\phi(E)$, and $\theta(E)$

$$\begin{aligned} &(S_{k,1}, S_{k,2}, \ldots, S_{k,M_k})^\tau \\ &(\phi_1, \phi_2, \ldots, \phi_{M_k})^\tau \\ &(\theta_1, \theta_2, \ldots, \theta_{M_k})^\tau \end{aligned} \quad (4)$$

where τ denotes the transpose of a vector or a matrix. Let

$$\boldsymbol{f} = (f_1, f_2, \ldots, f_J)^\tau, \quad \boldsymbol{g} = (g_1, g_2, \ldots, g_J)^\tau \quad (5)$$

denote the discrete form of $f(\boldsymbol{x})$ and $g(\boldsymbol{x})$ respectively, where f_j and g_j are the sampling values of $f(\boldsymbol{x})$ and $g(\boldsymbol{x})$ on the jth pixel, J is the total number of pixels of each image. Let $R_i = (r_{i1}, r_{i2}, \ldots, r_{iJ})$ be a projection vector, where r_{ij} represents the contribution of the jth pixel of $\boldsymbol{f}$ or $\boldsymbol{g}$ to the projec-

tion along the ith X-ray path. Generally, r_{ij} is selected to be the intersection length of the ith X-ray path with the jth pixel. With the above notations, we obtain the discrete form of polychromatic projections

$$p_{k,i} = -\ln \sum_{m=1}^{M_k} S_{k,m}\delta e^{-\phi_m R_i \boldsymbol{f} - \theta_m R_i \boldsymbol{g}}, \quad i \in \mathcal{I}_k, k = 1, 2 \tag{6}$$

where $\mathcal{I}_k$ indicates the index set of the X-ray paths corresponding to the kth spectrum. After discretization, the DSCT reconstruction problem is converted to solving $\boldsymbol{f}$ and $\boldsymbol{g}$ from (6), which is a nonlinear system.

B. Review of the ART Method

Standard CT reconstruction problem is usually modeled as a linear system

$$A\boldsymbol{x} = \boldsymbol{b} \tag{7}$$

where $A \in \mathbb{R}^{M\times N}$, $\boldsymbol{x}$ and $\boldsymbol{b}$ are N dimensional and M dimensional column vectors. The ART method [28] is an efficient iterative method for solving (7).

The ART method starts from some given initial values $\boldsymbol{x}^{(0)}$, and updates the estimated $\boldsymbol{x}$ by making use of the equations one by one. Suppose that we have known $\boldsymbol{x}^{(n)}$ after n iterations, and we are going to update the estimation according to the ith equation $A_i\boldsymbol{x} = b_i$, where A_i is the ith row of matix A. The iteration formula of the ART method is

$$\boldsymbol{x}^{(n+1)} = \boldsymbol{x}^{(n)} + \frac{b_i - A_i\boldsymbol{x}^{(n)}}{\|A_i\|}\frac{A_i^\tau}{\|A_i\|} \tag{8}$$

where $\|A_i\|$ is the l_2 norm of vector A_i.

In image reconstruction field, the calculation of $A_i\boldsymbol{x}^{(n)}$ from $\boldsymbol{x}^{(n)}$ is called forward projection, $b_i - A_i\boldsymbol{x}^{(n)}$ is called the residual, and adding back the weighted residual [with weight $(A_i^\tau)/(\|A_i\|^2)$] to $\boldsymbol{x}^{(n)}$ is called backprojection.

The iteration formula (8) has an obvious geometric explanation. In fact, each equation of the linear system (7) indicates a hyperplane in the N dimensional space $\mathbb{R}^N$, to solve the linear system is to find the intersections of these hyperplanes. Let H_i denote the hyperplane corresponding to the equation $A_i\boldsymbol{x} = b_i$; then $(A_i^\tau)/(\|A_i\|)$ in (8) denotes the unit normal of the hyperplane H_i, and $(b_i - A_i\boldsymbol{x}^{(n)})/(\|A_i\|)$ is the directed distance from the point $\boldsymbol{x}^{(n)}$ to the hyperplane H_i. So $\boldsymbol{x}^{(n+1)}$ is just the orthogonal projection of $\boldsymbol{x}^{(n)}$ on the hyperplane H_i. See Fig. 1(a) for an illustration.

C. The E-ART Method

In this subsection, we derive our E-ART method for DSCT. Each nonlinear equation of (6) indicates a hypersuface in space $\mathbb{R}^{2J}$. Therefore, to solve the nonlinear system is to find the intersections of these hypersurfaces. Suppose that we have estimation $(\boldsymbol{f}^{(n)}; \boldsymbol{g}^{(n)})$, where $(\boldsymbol{f}; \boldsymbol{g}) \triangleq (\boldsymbol{f}^\tau, \boldsymbol{g}^\tau)^\tau$, and we are going to update the estimation with

$$p_{k,i} = -\ln \sum_{m=1}^{M_k} S_{k,m}\delta e^{-\phi_m R_i \boldsymbol{f} - \theta_m R_i \boldsymbol{g}} \tag{9}$$

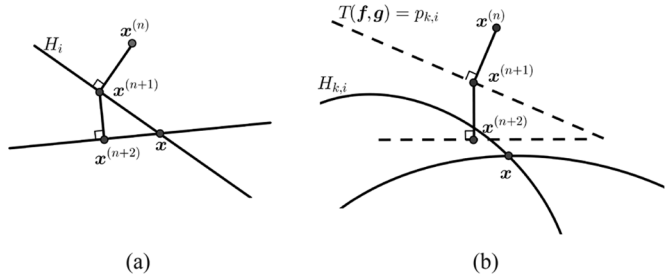

Fig. 1. Geometric illustration of (a) the ART method and (b) the proposed E-ART method for DSCT.

which corresponds to the hypersurface $H_{k,i}$. According to the idea of the ART method, we should calculate the orthogonal projection point of $(\boldsymbol{f}^{(n)}; \boldsymbol{g}^{(n)})$ to the hypersuface $H_{k,i}$ as the new estimation. But because of the nonlinearity of the right hand side of (9), it is difficult to calculate the orthogonal projection point. Therefore, we use a linear approximation to substitute the nonlinear equation (9), or in geometric words, we use a hyperplane to approximate the hypersurface.

After simple calculation, we obtain the first-order Taylor approximation at point $(\boldsymbol{f}^{(n)}; \boldsymbol{g}^{(n)})$ of the right-hand side of (9) as

$$\begin{aligned} T_{k,i}(\boldsymbol{f}, \boldsymbol{g}) &= p_{k,i}^{(n)} + \frac{\Phi_{k,i}^{(n)}}{q_{k,i}^{(n)}} R_i(\boldsymbol{f} - \boldsymbol{f}^{(n)}) + \frac{\Theta_{k,i}^{(n)}}{q_{k,i}^{(n)}} R_i(\boldsymbol{g} - \boldsymbol{g}^{(n)}) \\ &= p_{k,i}^{(n)} + \left(\frac{\Phi_{k,i}^{(n)}}{q_{k,i}^{(n)}} R_i, \frac{\Theta_{k,i}^{(n)}}{q_{k,i}^{(n)}} R_i\right) \begin{pmatrix} \boldsymbol{f} - \boldsymbol{f}^{(n)} \\ \boldsymbol{g} - \boldsymbol{g}^{(n)} \end{pmatrix} \end{aligned} \tag{10}$$

where

$$\begin{aligned} q_{k,i}^{(n)} &= \sum_{m=1}^{M_k} S_{k,m}\delta e^{-\phi_m R_i \boldsymbol{f}^{(n)} - \theta_m R_i \boldsymbol{g}^{(n)}} \\ p_{k,i}^{(n)} &= -\ln \sum_{m=1}^{M_k} S_{k,m}\delta e^{-\phi_m R_i \boldsymbol{f}^{(n)} - \theta_m R_i \boldsymbol{g}^{(n)}} \\ \Phi_{k,i}^{(n)} &= \sum_{m=1}^{M_k} S_{k,m}\delta\phi_m e^{-\phi_m R_i \boldsymbol{f}^{(n)} - \theta_m R_i \boldsymbol{g}^{(n)}} \\ \Theta_{k,i}^{(n)} &= \sum_{m=1}^{M_k} S_{k,m}\delta\theta_m e^{-\phi_m R_i \boldsymbol{f}^{(n)} - \theta_m R_i \boldsymbol{g}^{(n)}}. \end{aligned} \tag{11}$$

Then $p_{k,i} = T_{k,i}(\boldsymbol{f}, \boldsymbol{g})$, the linear approximation of the hypersurface $H_{k,i}$, can be expressed explicitly as

$$p_{k,i} = p_{k,i}^{(n)} + \left(\frac{\Phi_{k,i}^{(n)}}{q_{k,i}^{(n)}} R_i, \frac{\Theta_{k,i}^{(n)}}{q_{k,i}^{(n)}} R_i\right) \begin{pmatrix} \boldsymbol{f} - \boldsymbol{f}^{(n)} \\ \boldsymbol{g} - \boldsymbol{g}^{(n)} \end{pmatrix}. \tag{12}$$

We can calculate the orthogonal projection of $(\boldsymbol{f}^{(n)}; \boldsymbol{g}^{(n)})$ on the hyperplane corresponding to (12) as follows:

$$\begin{pmatrix} \boldsymbol{f}^{(n)} \\ \boldsymbol{g}^{(n)} \end{pmatrix} + \frac{(p_{k,i} - p_{k,i}^{(n)})}{\left\|\left(\frac{\Phi_{k,i}^{(n)}}{q_{k,i}^{(n)}} R_i, \frac{\Theta_{k,i}^{(n)}}{q_{k,i}^{(n)}} R_i\right)\right\|} \frac{\left(\frac{\Phi_{k,i}^{(n)}}{q_{k,i}^{(n)}} R_i, \frac{\Theta_{k,i}^{(n)}}{q_{k,i}^{(n)}} R_i\right)^\tau}{\left\|\left(\frac{\Phi_{k,i}^{(n)}}{q_{k,i}^{(n)}} R_i, \frac{\Theta_{k,i}^{(n)}}{q_{k,i}^{(n)}} R_i\right)\right\|}. \tag{13}$$

Similar to the ART method, we use this point as $(\boldsymbol{f}^{(n+1)};\boldsymbol{g}^{(n+1)})$. After simplification, we can rewrite the iteration formula of $\boldsymbol{f}^{(n+1)}$ and $\boldsymbol{g}^{(n+1)}$ as

$$\begin{aligned}\boldsymbol{f}^{(n+1)} &= \boldsymbol{f}^{(n)} + \frac{\Phi_{k,i}^{(n)}}{\left(\Phi_{k,i}^{(n)}\right)^2 + \left(\Theta_{k,i}^{(n)}\right)^2}\frac{R_i^T q_{k,i}^{(n)}(p_{k,i} - p_{k,i}^{(n)})}{|R_i|^2}\\ \boldsymbol{g}^{(n+1)} &= \boldsymbol{g}^{(n)} + \frac{\Theta_{k,i}^{(n)}}{\left(\Phi_{k,i}^{(n)}\right)^2 + \left(\Theta_{k,i}^{(n)}\right)^2}\frac{R_i^T q_{k,i}^{(n)}(p_{k,i} - p_{k,i}^{(n)})}{|R_i|^2}.\end{aligned} \tag{14}$$

In the iteration formula, (14), the calculation of $p_{k,i}^{(n)}$ according to (11) is called polychromatic forward projection, $p_{k,i} - p_{k,i}^{(n)}$ is called a residual, and adding the weighted residual back to $(\boldsymbol{f}^{(n)};\boldsymbol{g}^{(n)})$ is called backprojection. But different from the ART method, the forward projection step is nonlinear, and we need to calculate $q_{k,i}^{(n)}$, $\Phi_{k,i}^{(n)}$, and $\Theta_{k,i}^{(n)}$ at the same time.

Fig. 1(b) gives an illustration of our E-ART method. The dashed lines denote hyperplanes that are linear approximations of the hypersurfaces. The orthogonal projection of the current estimation on the hyperplane is regarded as the new estimation.

We summarize the implementation steps of the iteration scheme as follows.

Step 1. Assign $\boldsymbol{f}^{(0)}$ and $\boldsymbol{g}^{(0)}$ with some initial values.

Step 2. Suppose the estimations $\boldsymbol{f}^{(n)}$ and $\boldsymbol{g}^{(n)}$ are known after $n\ (\geq 0)$ iterations. For a given X-ray path along which the polychromatic projection is $p_{k,i}$, calculate $q_{k,i}^{(n)}$, $p_{k,i}^{(n)}$, $\Phi_{k,i}^{(n)}$, and $\Theta_{k,i}^{(n)}$ by (11).

Step 3. Calculate $\boldsymbol{f}^{(n+1)}$ and $\boldsymbol{g}^{(n+1)}$ by (14).

Step 4. Stop if the convergence criteria is satisfied, otherwise turn to Step 2.

IV. Numerical Experiments

In this section we perform some numerical experiments with simulated data to validate our E-ART method for DSCT. The basis material decomposition model is chosen in our experiments. The photoelectric/Compton effects model can be verified similarly. For simplicity, the numerical experiments are restricted to fan beam CT. Generalization to cone-beam CT is straightforward. As a comparison, we have also implemented the MDIR method because it is relatively new and practical.

A. Experiment Parameters and Conditions

1) X-ray Spectra and Mass Attenuation Coefficients: The polychromatic X-ray spectra are simulated with the software SpectrumGUI, an open source X-ray spectra simulator (see http://spectrumgui.sourceforge.net/). We have simulated the X-ray spectra of GE Maxiray 125 X-ray tube with tube voltages 80 and 140 kV, where the latter one is filtered with 1 mm copper. The distributions of the X-ray spectra are shown in Fig. 2.

The mass attenuation coefficients used in the experiments are retrieved from the National Institute of Standard Technology (NIST) tables of X-ray mass attenuation coefficient [27].

2) Scanning Configuration: The parameters of the scanning configuration are set as follows: the distance from the X-ray source to the rotation center is 1000 mm, and the distance from the X-ray source to the linear detector is 1200 mm. These two

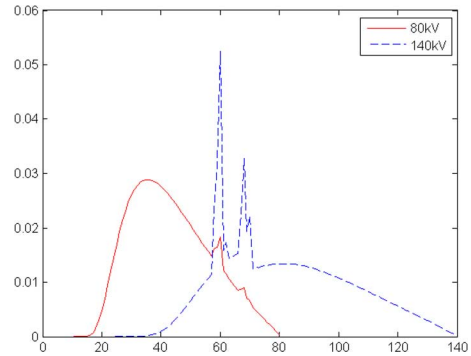

Fig. 2. X-ray spectra used in the numerical experiments.

Fig. 3. Forbild head phantom used in the numerical experiments.

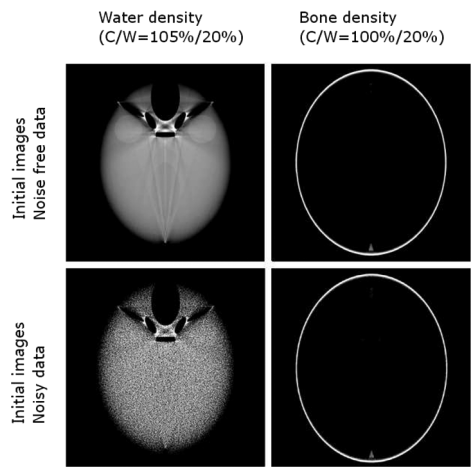

Fig. 4. Initial images for the MDIR method and the proposed E-ART method.

parameters are set referring to the experimental CT system of our laboratory. The linear detector is composed of 1024 detector cells, and the length of each cell is 0.3 mm. The cell size is selected to accommodate a proper field of view. With the above parameters, the diameter of the field of view is 256 mm.

Projections corresponding to different X-ray spectra are acquired in an alternate manner, i.e., projections are geometrically inconsistent. 720 projections are simulated on one full turn for each spectrum.

3) Phantom: The phantom used in the numerical experiments is a slice of the 3-D forbild head phantom without ears,

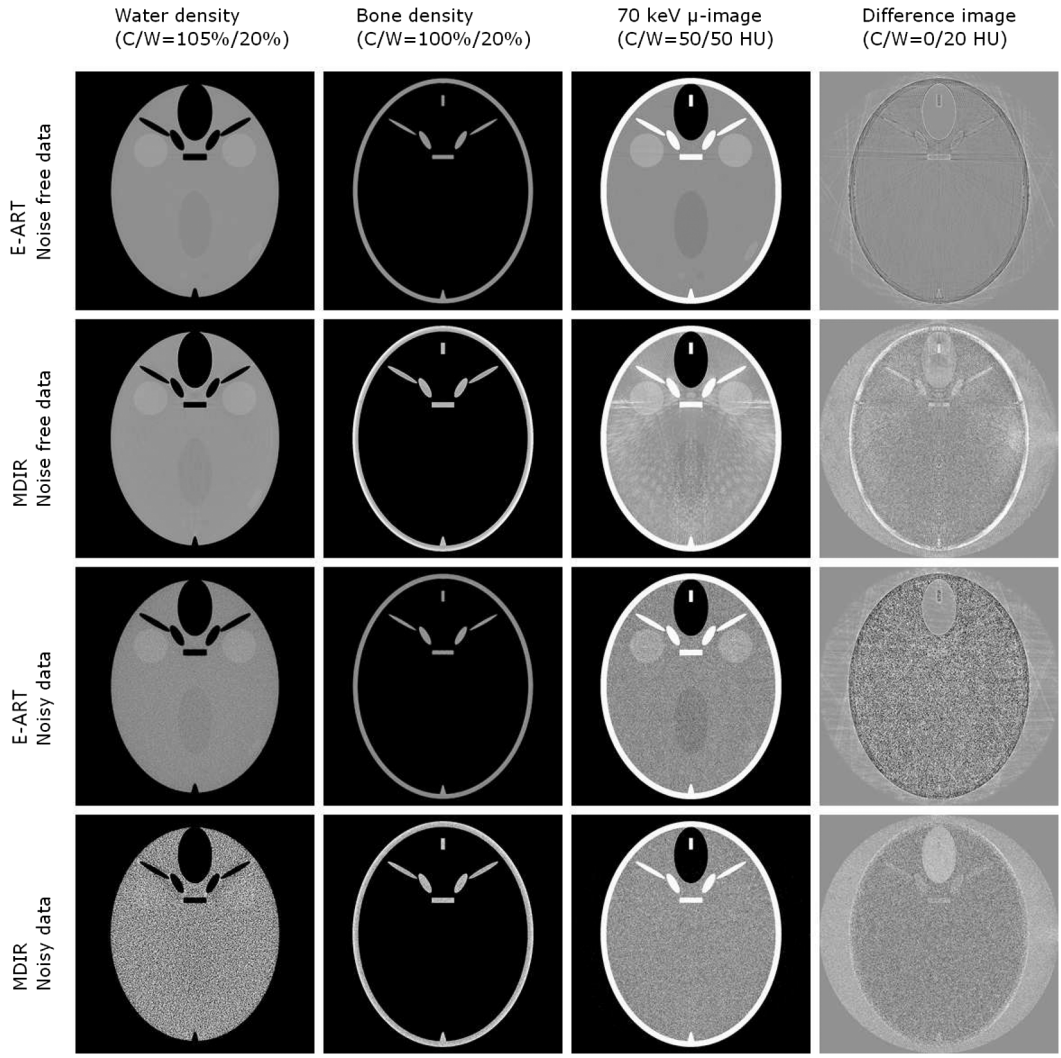

Fig. 5. Results reconstructed with our E-ART method and the MDIR method.

which is shown in Fig. 3. Geometric information and the reference materials of different part of the phantom are detailed on its web site [29]. The MDIR method needs a calibration phantom to get the maps from polychromatic projections to the line integrals of basis materials. In order to get a better reconstruction results we use the head phantom itself as the calibration phantom.

4) Implementation Details: The polychromatic projections are simulated according to

$$p_{k,i} = -\ln \sum_{m=1}^{M_k} S_{k,m}\delta e^{-\sum_{n=1}^{N}\mu_{n,m}l_{n,i}}, \quad i \in \mathcal{I}_k, k = 1, 2 \tag{15}$$

where N is the number of materials composing the phantom, $\mu_{n,m}$ is the sampling value of the mass attenuation coefficient of the nth material at the mth sampling subinterval of energy (the length of the sampling subinterval δ is 1 keV in the simulation of polychromatic projections), $l_{n,i}$ is the intersection length of the ith X-ray path with the nth material, which is calculated analytically according to the definition of the phantom. We simulate both noise free data and Poisson noise data corresponding to emission flux of 10^6 photons per measurement.

In image reconstruction, we choose water and bone as the two basis materials. The size of all the images reconstructed is 1024×1024. We use the results of an image based reconstruction method, which is shown in Fig. 4, as the initial values for

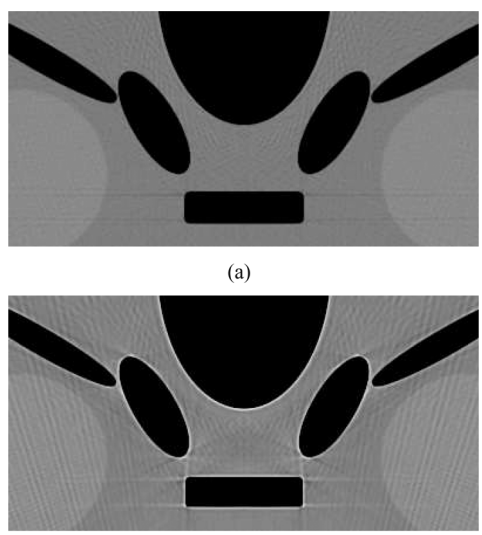

(a)

(b)

Fig. 6. Zoom in images of part of the noise free water density images shown in Fig. 5. (a) E-ART method result and (b) MDIR result.

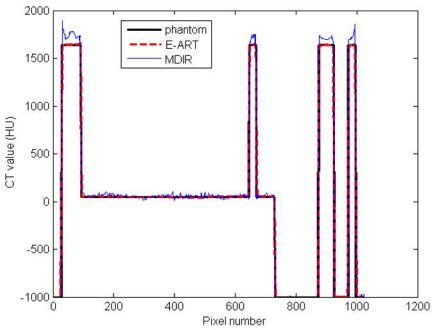

(a)

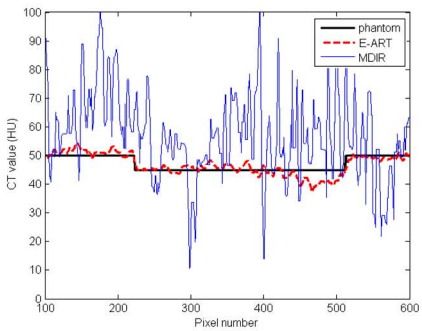

(b)

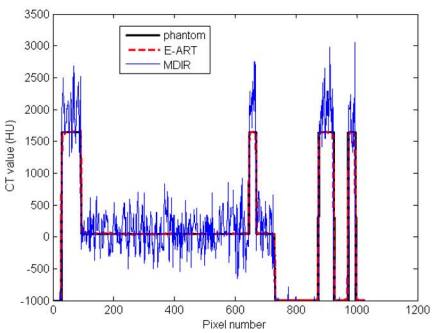

(c)

Fig. 7. Profiles of the central columns of the monochromatic images shown in Fig. 5. (a) Profile of the images reconstructed from noise free data. (b) Zoom in display of part of the profile shown in (a). (c) Profile of the images reconstructed from noisy data.

both the MDIR method and the proposed E-ART method. The iteration is stopped after 10 round of iterations. One round of iterations we refer here means all projections have been used once.

In the implementation of proposed E-ART method, a ray casting method is used in the forward projection and a pixel driven method is used in backprojection, which make the method suitable for acceleration on GPUs (graphic processing units) or other parallel systems. For the detailed information of the two techniques, please refer to [30]. The numerical experiments is carried out on a DELL workstation with a 1.83 GHz Intel Xeon 5120 dual-core CPU, 8 GB system memory, and a NVIDIA Quadro FX 5600 graphics card with 1.5 GB video memory. The codes are written in C++ and CUDA (An application programming interface provided by NVIDIA) [31].

TABLE I
TWO DISTANCE MEASURES FOR THE MONOCHROMATIC IMAGES SHOWN IN FIG. 5

	NMSD		NMAD	
	Noise free	Noisy	Noise free	Noisy
E-ART result	0.106745	0.108124	0.019873	0.025326
MDIR result	0.106932	0.158437	0.038354	0.113275

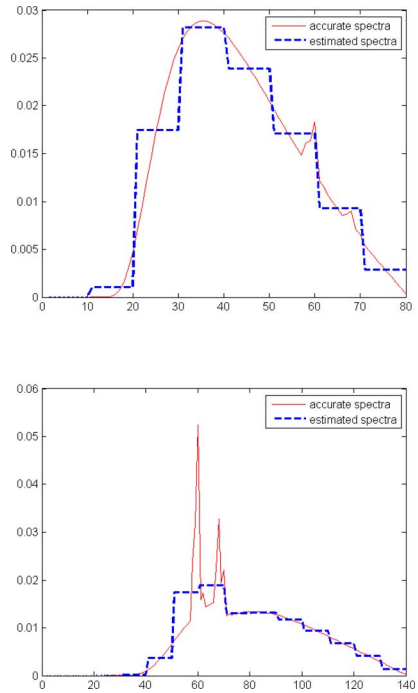

Fig. 8. Estimated and accurate X-ray spectra.

B. Reconstruction Results

1) Reconstruction With Ideal X-ray Spectra: In this case, we use the same X-ray spectra and sampling subinterval of energy as those used in the simulation of the polychromatic projections.

Fig. 5 shows the results reconstructed with our E-ART method and the MDIR method from noise free data and noisy data. The first and the third rows are the results of our E-ART method from noise free and noisy data, respectively. The second and the fourth rows are the results of the MDIR method from noise free and noisy data, respectively.

Fig. 6 shows the zoom in images of part of the noise free water density images shown in Fig. 5.

Fig. 7 shows the profiles of the central columns of the monochromatic images shown in Fig. 5. The left one is the profile of the images reconstructed from noise free data, the middle one is a zoom in display of low contrast part of the left profile, and the right one is the profile of the images reconstructed from noisy data. We calculate the normalized mean square distance (NMSD) and the normalized mean absolute distance (NMAD) [11] of the monochromatic images shown in Fig. 5 and the values are shown in Table I.

We can see from Figs. 5–7, and Table I that the results reconstructed with our E-ART method are superior to those reconstructed with the MDIR method in general. First, there are shadow and strick artifacts shown in the water density image

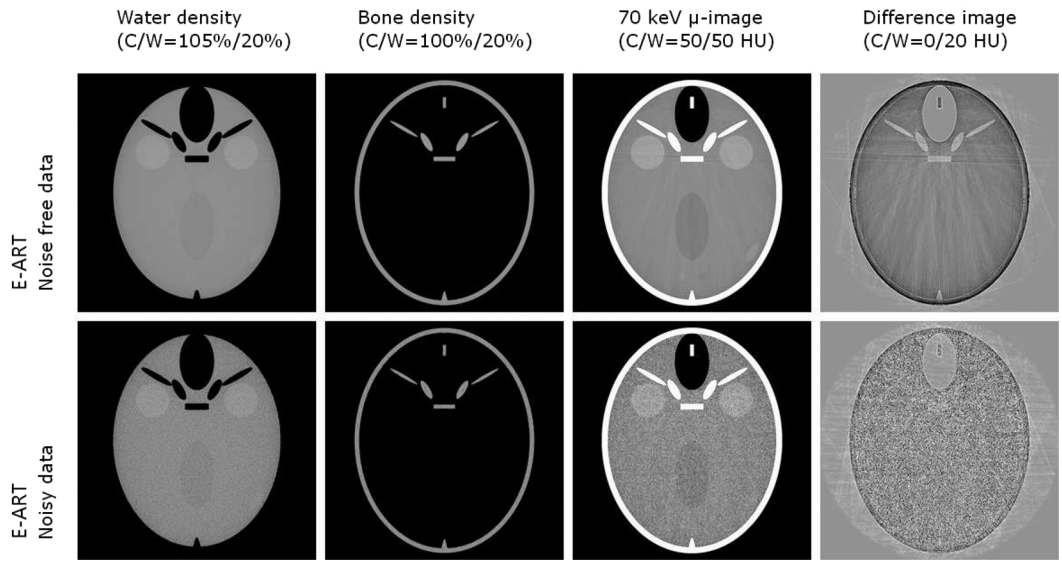

Fig. 9. Results reconstructed with our E-ART method using estimated X-ray spectra.

TABLE II
TWO DISTANCE MEASURES FOR THE MONOCHROMATIC IMAGES SHOWN IN FIG. 9

	NMSD		NMAD	
	Noise free	Noisy	Noise free	Noisy
E-ART method estimated spectra	0.106885	0.109364	0.021362	0.027483

reconstructed with the MDIR from noise free data, while there are no evident shadow and strick artifacts in the images reconstructed with our E-ART method (see the two images shown in Fig. 6). Second, the low contrast components of the phantom can be distinguished in the images reconstructed with our E-ART method from noisy data (see the first and the third images in the third row of Fig. 5), but the same low contrast components cannot be distinguished in the images reconstructed with the MDIR method from noisy data (see the first and the third images in the last row of Fig. 5).

2) Reconstruction With Estimated X-ray Spectra: In the following, we test the tolerance of our method to the errors in the X-ray spectra.

To our knowledge, there are several methods to estimate the X-ray spectrum of an X-ray tube [24], [25], [32]. We estimate the X-ray spectra from transmission measurements simply by first solving a linear system and then setting negative values to zeros. The length of the sampling subinterval of energy is 10 keV, 10 times bigger than that used in the simulation of projections. The estimated X-ray spectra are inferior to those estimated with the methods mentioned above. Fig. 8 shows the accurate X-ray spectra and their estimations. There are obvious differences between the estimated X-ray spectra and the accurate ones.

Fig. 9 shows the images reconstructed with our E-ART method using the estimated X-ray spectra. Table II shows the two measures for the monochromatic images shown in Fig. 9. It follows from the images in Fig. 9 and the two measures of NMSD and NMAD that our method has a well tolerance to the errors in the estimated X-ray spectra.

V. SUMMARY

In this paper, we have proposed a model to depict the DSCT reconstruction problem, and proposed the E-ART method for solving the problem. Numerical experiments verify its validity. High quality images are reconstructed with our E-ART method from the polychromatic projections of DSCT. The reconstructed images are still satisfactory even if there are certain errors in the estimated X-ray spectra.

We have tested several other phantoms, which are not listed in this manuscript because of space constraints, to verify the convergence of the proposed method, and all give positive results. The proof of the convergence of the proposed method is also interesting theoretically and will be studied further.

In the derivation of the E-ART method, we have restricted our discussion in the case with two X-ray spectra and two basis materials. But from the iteration formulae, we can see that the iteration can be carried out as long as the X-ray spectra and the mass attenuation coefficients of the basis materials are known. So our E-ART method is not only applicable to dual spectral CT but also applicable to multiple spectral CT (slow kVp switching CT, for example) and multiple basis material decomposition case.

ACKNOWLEDGMENT

The authors would like to thank Dr. Clements Maaß for his instructions on the implementation of the MDIR method and his constructive suggestions on the modification of the manuscript. We thank Dr. Huitao Zhang for his helpful discussion.

REFERENCES

[1] S. J. Riederer and C. A. Mistretta, "Selective iodine imaging using K-edge energies in computerized X-ray tomography," *Med. Phys.*, vol. 4, no. 6, pp. 474–481, 1977.
[2] R. Alvarez and A. Macovski, "Energy-selective reconstructions in X-ray computerised tomography," *Phys. Med. Biol.*, vol. 21, no. 5, pp. 733–744, 1976.
[3] R. Alvarez and E. Seppi, "A comparison of noise and dose in conventional and energy selective computed tomography," *IEEE Trans. Nucl.*, vol. 26, no. 2, pp. 2853–2856, 1979.
[4] W. A. Kalender, W. H. Perman, J. R. Vetter, and E. Klotz, "Evaluation of a prototype dual-energy computed tomographic apparatus. I. Phantom studies," *Med. Phys.*, vol. 13, no. 3, pp. 334–339, 1986.

[5] J. R. Vetter, W. H. Perman, W. A. Kalender, R. B. Mazess, and J. E. Holden, "Evaluation of a prototype dual-energy computed tomographic apparatus. II. Determination of vertebral bone mineral content," *Med. Phys.*, vol. 13, no. 3, pp. 340–343, 1986.

[6] K. Chuang and H. K. Huang, "Comparison of four dual energy image decomposition methods," *Phys. Med. Biol.*, vol. 33, no. 4, pp. 455–466, 1988.

[7] G. Zhang, Z. Chen, L. Zhang, and J. Cheng, "Exact reconstruction for dual energy computed tomography using an H-L curve method," pp. 3485–3488, 2006, IEEE.

[8] J. Fessler, I. Elbakri, P. Sukovic, and N. Clinthorne, "Maximum-likelihood dual-energy tomographicimage reconstruction," in *Proceedings of SPIE Medical Imaging*, 2002, vol. 4684, no. 1, pp. 38–49, spie.

[9] R. A. Brooks and G. D. Chiro, "Beam hardening in X-ray reconstructive tomography," *Phys. Med. Biol.*, vol. 21, no. 3, pp. 390–398, 1976.

[10] A. J. Coleman and M. Sinclair, "A beam-hardening correction using dual-energy computed tomography," *Phys. Med. Biol.*, vol. 30, no. 11, pp. 1251–1256, 1985.

[11] G. Herman, *Fundamentals of Computerized Tomography: Image Reconstruction From Projections*. : Springer Verlag, 2009, vol. 11, no. 1.

[12] F. Noo, R. Clackdoyle, and J. Pack, "A two-step hilbert transform method for 2D image reconstruction," *Phys. Med. Biol.*, vol. 49, no. 17, pp. 3903–3923, 2004.

[13] C. Maaß, E. Meyer, and M. Kachelrieß, "Exact dual energy material decomposition from inconsistent rays (MDIR)," *Med. Phys.*, vol. 38, no. 2, pp. 691–700, 2011.

[14] T. Flohr *et al.*, "First performance evaluation of a dual-source CT (DSCT) system," *European Radiology*, vol. 16, no. 2, pp. 256–268, 2006.

[15] M. Petersilka, H. Bruder, B. Krauss, K. Stierstorfer, and T. Flohr, "Technical principles of dual source CT," *Eur. J. Radiol.*, vol. 68, no. 3, pp. 362–368, 2008.

[16] Q. Xu, X. Mou, S. Tang, W. Hong, Y. Zhang, and T. Luo, "Implementation of penalized-likelihood statistical reconstruction for polychromatic dual-energy CT," in *Proceedings of SPIE*, 2009, vol. 7258, p. 72585I.

[17] I. A. Elbakri and J. A. Fessler, "Statistical image reconstruction for polyenergetic X-ray computed tomography," *IEEE Trans. Med. Imag.*, vol. 21, no. 2, pp. 89–99, 2002.

[18] P. Sukovic and N. H. Clinthorne, "Penalized weighted least-squares image reconstruction for dual energy X-ray transmission tomography," *IEEE Trans. Med. Imag.*, vol. 19, no. 11, pp. 1075–1081, 2000.

[19] C. Maaß, R. Grimmer, and M. Kachelries, "Dual energy CT material decomposition from inconsistent rays (MDIR)," in *Nuclear Science Symposium Conference Record (NSS/MIC), 2009 IEEE*, 2009, pp. 3446–3452, IEEE.

[20] T. P. Szczykutowicz and G. H. Chen, "Dual energy CT using slow kVp switching acquisition and prior image constrained compressed sensing," *Phys. Med. Biol.*, vol. 55, no. 21, pp. 6411–6429, 2010.

[21] J. Schlomka *et al.*, "Experimental feasibility of multi-energy photon-counting K-edge imaging in pre-clinical computed tomography," *Physics in Medicine and Biology*, vol. 53, no. 15, p. 4031, 2008.

[22] X. Liu, L. Yu, A. N. Primak, and C. H. McCollough, "Quantitative imaging of element composition and mass fraction using dual-energy CT: Three-material decomposition," *Medical Physics*, vol. 36, no. 5, pp. 1602–1609, 2009.

[23] C. Yan, R. Whalen, G. Beaupre, S. Yen, and S. Napel, "Reconstruction algorithm for polychromatic CT imaging: Application to beam hardening correction," *IEEE Trans. Med. Imag.*, vol. 19, no. 1, pp. 1–11, 2000.

[24] E. Sidky, L. Yu, X. Pan, Y. Zou, and M. Vannier, "A robust method of X-ray source spectrum estimation from transmission measurements: Demonstrated on computer simulated, scatter-free transmission data," *J. Appl. Phys.*, vol. 97, no. 12, p. 124701, 2005.

[25] X. Duan, J. Wang, L. Yu, S. Leng, and C. McCollough, "CT scanner X-ray spectrum estimation from transmission measurements," *Med. Phys.*, vol. 38, no. 2, pp. 993–997, 2011.

[26] Y. Yang, X. Mou, and X. Chen, "A robust X-ray tube spectra measuring method by attenuation data," in *Proceedings of SPIE*, 2006, vol. 6142, p. 61423K.

[27] J. H. Hubbell and S. M. Seltzer, Tables of X-ray Mass Attenuation Coefficients and Mass Energy-Absorption Coefficients 1 keV to 20 MeV for Elements Z = 1 to 92 and 48 Additional Substances of Dosimetric Interest Ionizing Radiation Div., National Inst. of Standards and Technology-PL, Gaithersburg, MD, United States, Tech. Rep., 1995.

[28] R. Gordon, R. Bender, and G. T. Herman, "Algebraic reconstruction techniques (ART) for three-dimensional electron microscopy and X-ray photography.," *J. Theor. Biol.*, vol. 29, no. 3, pp. 471–481, 1970.

[29] Forbild Head Phantom Homepage 2012 [Online]. Available: http://www.imp.uni-erlangen.de/forbild/deutsch/results/head/head.html, [Online]. Available:

[30] X. Zhao, J. Bian, E. Sidky, S. Cho, P. Zhang, and X. Pan, "GPU-based 3D cone-beam CT image reconstruction: Application to micro CT," in *Nuclear Science Symposium Conference Record, 2007. NSS'07. IEEE*, 2007, vol. 5, pp. 3922–3925, IEEE.

[31] CUDA Homepage 2013, [Online]. Available: [Online]. Available: http://www.nvidia.com/object/cuda_home_new.html

[32] D. Xu, D. Langan, X. Wu, J. Pack, T. Benson, J. Tkaczky, and A. Schmitz, "Dual energy CT via fast kVp switching spectrum estimation," in *Proc. SPIE*, 2009, vol. 7258, p. 72583T.